Cellular/Molecular

Long-Lasting, Pathway-Specific Impairment of a Novel Form of Spike-Timing-Dependent Long-Term Depression by Neuropathic Pain in the Anterior Cingulate Cortex

Norbert Hogrefe, Sigrid M. Blom, Kristina Valentinova, Niels R. Ntamati, Lotte J.E. Jonker, Natalie E. Nevian, and Thomas Nevian

Department of Physiology, University of Bern, 3012 Bern, Switzerland

Malfunctioning synaptic plasticity is one of the major mechanisms contributing to the development of chronic pain. We studied spike-timing dependent depression (tLTD) in the anterior cingulate cortex (ACC) of male mice, a brain region involved in processing emotional aspects of pain. tLTD onto layer 5 pyramidal neurons depended on postsynaptic calcium-influx through GluN2B-containing NMDARs and retrograde signaling via nitric oxide to reduce presynaptic release probability. After chronic constriction injury of the sciatic nerve, a model for neuropathic pain, tLTD was rapidly impaired; and this phenotype persisted even beyond the time of recovery from mechanical sensitization. Exclusion of GluN2B-containing NMDARs from the postsynaptic site specifically at projections from the anterior thalamus to the ACC caused the tLTD phenotype, whereas signaling downstream of nitric oxide synthesis remained intact. Thus, transient neuropathic pain can leave a permanent trace manifested in the disturbance of synaptic plasticity in a specific afferent pathway to the cortex.

Key words: **anterior cingulate cortex; neuropathic pain; synaptic plasticity**

Significance Statement

Synaptic plasticity is one of the main mechanisms that contributes to the development of chronic pain. Most studies have focused on potentiation of excitatory synaptic transmission, but very little is known about the reduction in synaptic strength. We have focused on the ACC, a brain region associated with the processing of emotional and affective components of pain. We studied spike-timing dependent LTD, which is a biologically plausible form of synaptic plasticity, that depends on the relative timing of presynaptic and postsynaptic activity. We found a long-lasting and pathway-specific suppression of the induction mechanism for spike-timing dependent LTD from the anterior thalamus to the ACC, suggesting that this pathology might be involved in altered emotional processing in pain.

Introduction

Synaptic plasticity is an essential process in the development of chronic pain. Strong activation of the nociceptive sensory system, after nerve damage or inflammation, results in the sensitization of synaptic transmission at all stages along the nociceptive pathway contributing to the chronification of pain. LTP at peripheral nociceptive afferent synapses onto projection neurons in the spinal cord is an initial key mechanism for central sensitization of the nociceptive system (Sandkuhler, 2000; Woolf and Salter, 2000; Basbaum et al., 2009). Synaptic plasticity mechanisms in supraspinal pain areas also contribute significantly to the development of chronic pain (Kuner, 2010). LTP induces increased synaptic transmission in several cortical regions in animal models of chronic pain, including the somatosensory cortex and the ACC (Xu et al., 2008; Zhuo, 2008; Bliss et al., 2016). Particularly, plasticity in the ACC, a brain region that is fundamentally associated with the emotional and affective processing of pain (Santello et al., 2017; Kasanetz and Nevian, 2021), has been functionally linked to some comorbid symptoms of chronic pain like anxiety and depression (Koga et al., 2015; Sellmeijer et al., 2018). Thus, LTP mechanisms might contribute to the altered responsiveness of the ACC in chronic pain.

LTD has also been found to be affected in the ACC during chronic pain syndromes. The development and maintenance of bone cancer pain are associated with a persistent decrease in NMDAR expression and a functional loss of LTD in L2/3 pyramidal neurons of the ACC (Chiou et al., 2012). ACC LTD was also

Received Feb. 11, 2021; revised Dec. 30, 2021; accepted Jan. 18, 2022.

Author contributions: N.H., S.M.B., K.V., N.E.N., L.J.E.J., N.R.N., and T.N. designed research; N.H., S.M.B., K.V., N.R.N., L.J.E.J., and N.E.N. performed research; N.H., S.M.B., K.V., N.R.N., L.J.E.J., N.E.N., and T.N. analyzed data; N.H. and T.N. wrote the first draft of the paper; N.H., K.V., N.R.N., L.J.E.J., N.E.N., and T.N. edited the paper; N.H. and T.N. wrote the paper.

This work was supported by Swiss National Science Foundation Grants 128415, 159872, and 182571 to T.N.; and European Research Council Grant 682905 to T.N.

The authors declare no competing financial interests.

Correspondence should be addressed to Thomas Nevian at thomas.nevian@unibe.ch.

https://doi.org/10.1523/JNEUROSCI.0326-21.2022

impaired in adult rats with single-digit amputation (Wei et al., 1999) and in mice with tail amputation (Kang et al., 2012), models that mimic phantom limb pain. In these studies, LTD was induced by low-frequency synaptic stimulation that only depended on the presynaptic spiking pattern. LTD can also be induced by the precise temporal pairing of presynaptic and postsynaptic activity. The timing between the presynaptic and postsynaptic spikes has been found to be an important determinant for the direction and magnitude of changes in synaptic strength (Markram et al., 1997; Sjostrom et al., 2001; Bender et al., 2006; Dan and Poo, 2006; Nevian and Sakmann, 2006). A postsynaptic action potential (AP) that follows a presynaptic AP within a critical time window of 10-40 ms results in LTP, whereas the reverse order results in LTD, a notion termed spike timing-dependent plasticity (Bi and Poo, 1998). Spike timing-dependent plasticity is considered as a plausible mechanism for synaptic modifications in brain areas in which spiking activity is sparse and information is coded in the relative timing between presynaptic and postsynaptic activity. Mechanistically, spike-timing dependent LTD (tLTD) often requires the involvement of a retrograde messenger. At L2/3 and L5 synapses in the somatosensory and visual cortices, coincident activation of metabotropic glutamate receptors (mGluRs) and voltage-gated Ca^{2+} channels leads to activation of PLC, resulting in the generation and release of endocannabinoids from the postsynaptic compartment (Sjostrom et al., 2001; Bender et al., 2006; Nevian and Sakmann, 2006). The endocannabinoids activate astrocytes that release glutamate onto presynaptic NMDARs (Min and Nevian, 2012), which are essential in the signaling cascade to downregulate release probability involving calcineurin (Rodriguez-Moreno et al., 2013; Neubauer et al., 2022).

Nitric oxide (NO) can also function as a retrograde messenger in synaptic plasticity (Hardingham et al., 2013). In the brain, NO is produced from L-arginine by the Ca^{2+}/calmodulin-dependent neuronal NO synthase (nNOS) (Garthwaite, 2008). The necessary Ca^{2+} signal for NO production is believed to originate from activation of NMDARs, as nNOS is anchored to the NMDAR through mutual interactions with PSD-95 (Christopherson et al., 1999). Most often retrograde synaptic NO signaling results in the expression of LTP, but it can also be involved in LTD induction. Most prominently, this has been shown at the parallel fiber to Purkinje cell synapse in the cerebellum (Casado et al., 2000). But NO can also be involved in LTD at cortical synapses, where it activates soluble guanylyl cyclase and protein kinase G (PKG)-dependent mechanisms to modulate presynaptic release (Huang and Hsu, 2010).

Understanding the differences between the plasticity mechanisms in cortical pain processing areas like the ACC is important to design novel pharmacological treatment strategies to specifically target cortical pain perception without interfering with other sensory modalities. In order to manipulate synaptic plasticity in a therapeutically meaningful way, the layer- and cell type-specific mechanisms have to be revealed. L5 pyramidal neurons in the ACC are of particular interest as they integrate a multitude of inputs and send this information to cortical and subcortical areas, including the periaqueductal gray, an area that plays an important role in the descending modulation of pain (Calejesan et al., 2000; Ossipov et al., 2014).

Here, we investigated whether neuropathic pain induced by chronic constriction injury (CCI) affected tLTD in L5 of the ACC. We found that tLTD was absent in mice with CCI. Dissection of the underlying signaling cascade revealed the essential involvement of postsynaptic GluN2B-containing NMDARs and retrograde NO signaling in tLTD. Examining the potentially affected afferents with channelrhodopsin-assisted circuit tracing revealed that specifically the inputs from the anterior thalamic nuclei (ATN), a relay region in the thalamus that is part of the limbic system for emotional processing, lost their ability for tLTD. The loss of tLTD had a rapid onset after CCI and was persistent even after mechanical sensitivity of the injured hindpaw had recovered at ~5 weeks after surgery in a subgroup of animals. Thus, our results suggest that nerve injury has long-term effects on pathway specific synaptic plasticity mechanisms in the ACC even beyond the time of healing.

Materials and Methods

All experiments were conducted in accordance to the rules of the veterinary office of the canton of Bern (Switzerland). For all experiments, adult male mice of the C57/BL6 strain were used. Animals were housed under a 12/12 h light-dark cycle in cages containing 2-5 littermates.

Brain slice preparation and electrophysiology. Animals (8-17 weeks) were deeply anesthetized with isoflurane (2%-2.5%). After decapitation, brains were removed rapidly and transferred to ice-cold slicing solution composed of the following (in mM): 65 NaCl, 2.5 KCl, 1.25 NaH_2PO_4, 25 $NaHCO_3$, 7 $MgCl_2$, 0.5 $CaCl_2$, 5 glucose, and 105 sucrose, and then mounted inside a slicing chamber containing the same ice-cold solution. After preparing coronal slices (300 µm) using a vibratome (HM 650, Microm, Thermo Fisher Scientific), slices recovered in ACSF containing the following (in mM): 125 NaCl, 2.5 KCl, 1.25 NaH_2PO_4, 25 $NaHCO_3$, 1 $MgCl_2$, 2 $CaCl_2$, and 25 glucose at 34°C, and after 30 min they were transferred to room temperature. Slicing solution and ACSF were saturated with 95% O_2 and 5% CO_2 throughout the entire procedure and experiment.

For experiments, slices containing the rostroventral ACC (1.0-1.5 mm below the pial surface, 1.1-0.2 mm rostral to bregma) were transferred to a chamber with continuous flow of ACSF (30°C-32°C) and somatic whole-cell patch-clamp recordings were performed on layer 5 pyramidal neurons in the right hemisphere (Santello and Nevian, 2015). Cells had on average a resting membrane potential of -70.6 ± 1.4 mV and an input resistance of 88.2 ± 7.6 MΩ ($n = 18$). Patch pipettes were made from borosilicate glass capillaries, and target cells were identified using a Leica Microsystems DMLFSA microscope (40× water-immersion objective) based on their size, a clearly visible apical dendrite, and the detection of a voltage sag on injection of a hyperpolarizing current. Recordings were performed using a BVC-700A amplifier (Dagan), and data were acquired with an ITC-16 board (Instrutech) and IGOR software (Wavemetrics). For current-clamp experiments patch pipettes with a resistance of 4-7 MΩ were filled with intracellular solution containing the following (in mM): 130 K-gluconate, 5 KCl, 10 HEPES, 10 Na-PO_4-creatine, 4 Mg-ATP, 0.3 Na-GTP, and 0.2% biocytin, pH 7.3. For experiments in which intracellular calcium levels were clamped at a physiological concentration (Ca^{2+}-clamp), the same intracellular solution was used, except that 15 mM BAPTA (as K_4-salt) and 1.5 mM Ca^{2+} were added and K-gluconate was lowered in concentration (Nabavi et al., 2013). Sucrose (15 mM) was added to compensate for a change in osmolarity.

To evoke EPSPs in the patched pyramidal neuron, a bipolar glass stimulation electrode, prepared from Clark borosilicate theta-glass pulled to a thin opening on a horizontal puller, was used, filled with ACSF and placed at the border of layer 2/3 to layer 5 (Nevian and Sakmann, 2004). After recording of a stable baseline for 10 min at 0.1 Hz stimulation, timing-dependent LTD was induced by pairing an EPSP with one preceding postsynaptic AP (Δt (post-pre) = −25 ms). This pairing paradigm was repeated 60× at 0.1 Hz. After the pairing period, EPSPs were recorded for an additional 50 min. To evaluate for changes in synaptic strength, the average EPSP amplitude between minutes 20 and 40 was compared with the average of the baseline. Throughout the entire experiment, input resistance (calculated from the response to a hyperpolarizing current step during each sweep) and resting membrane potential were monitored, and recordings were discarded if at least one changed >20%. An unstable baseline (first 15 EPSP amplitudes changed

>20% compared with last 15) was another criterion to exclude experiments from further analysis. At the end of the recording, pipettes were slowly retracted, and slices were transferred to a glass vial containing PBS with 4% PFA for fixation and for morphologic recovery of the patched cell. To stain the cells, the avidin-biotin-peroxidase method was used (Egger et al., 2008; Sieber et al., 2013) and slices were mounted on cover slides for further processing.

To study AMPAR and NMDAR functioning, pyramidal neurons were recorded in voltage-clamp mode and patch pipettes with a resistance of 2-5 MΩ were filled with an intracellular solution containing the following (in mM): 130 gluconic acid, 130 CsOH, 5 KCl, 10 HEPES, 10 phosphocreatine, 4 Mg^{2+}-ATP, 0.3 GTP, and 0.1 spermine. After establishing the whole-cell configuration, cells were clamped at −60 mV (not corrected for liquid junction potential) for 10 min to allow for equilibration of internal solution. A bipolar stimulation pipette placed at the border of layer 2/3 to layer 5 was used to evoke EPSCs in the patched neuron at a frequency of 0.1 Hz. The last 20-30 sweeps of a protocol were used to calculate the EPSC average before changing the holding potential or washing-in a drug.

Optogenetic stimulation of axons expressing ChR-2 was performed through the objective (HCX APO w40x UVI, NA 0.75, Leica Microsystems) with blue light (470 nm, 5 ms) from a collimated LED light source (M470L4-C2, Thorlabs) attached to the epifluorescence port of the microscope (DMLFSA, Leica Microsystems). Depending on the experiment, light-evoked EPSPs or EPSCs were recorded from L5 pyramidal neurons in the ACC (Marti Mengual et al., 2020).

CCI and von Frey testing. To study the effects of neuropathic pain, the CCI model was used as described previously (Blom et al., 2014). Mice were anesthetized with isoflurane (1%-1.5%), vaporized with 100% oxygen, and operated under a sterile hood on a heating pad keeping body temperature at 36°C. To protect the eyes from drying out, eye ointment (Pharma Medica) was applied. Fur on the left leg was shaved using depilatory cream, and an incision was performed with a scalpel. The sciatic nerve was exposed by separating and keeping apart the two muscles above with a small tissue retractor (Fine Science Tools). Sterile sofsilk thread 5–0 (Coviden) was cast around the nerve to make three loose ligations (~1 mm apart). The skin was then sutured with an absorbable thread (4–0 coated Vicryl rapid suture, Ethicon), and animals could recover from the operation under supervision. Sham animals were operated the very same way, except that no ligations were performed.

An electronic VON FREY anesthesiometer (IITC Life Science) was used to test mice for mechanical hypersensitivity. For this, mice were habituated for 15-30 min on a metal grid under a plastic box. Then, a von Frey filament was carefully pressed to the midplantar surface of the hindpaw until the paw was withdrawn. This procedure was performed 6× per each paw; and via an unpaired *t* test, exclusion or inclusion of the animal was decided. For electrophysiology experiments, all animals were tested at least at two time points before and after the surgery. Those animals used for studying long-term effects of neuropathic pain were subjected to the von Frey test for 5 weeks with three measurements per week. To decide at the end of the 5 weeks whether an animal which underwent the CCI surgery still exhibited mechanical hypersensitivity or not, the last three von Frey tests were used. If at least two of the three tests did not show a significant difference between the left and the right paw, the animal was counted as recovered; otherwise, it was counted as still hypersensitive.

Stereotactic injections. Mice (4-6 weeks) were anesthetized with isoflurane (1%-1.5%) and mounted in a head holder of a stereotactic frame (Leica Biosystems). Glass pipettes (Blaubrand, Brand) were connected to the microinjector Picospritzer III (Parker Hannifin), and 100 nl of virus solution were injected, except for injections into the retrosplenial cortex (RSC) where 200 nl were injected within 3-4 min and for the injections into the ACC of the right hemisphere where 75 nl were injected within 1 min.

To express channelrhodopsin, animals were injected with rAAV2-CaMKIIa-hChR2(H134R)-mCherry (UNC Vector Core) in the right hemisphere in the mediodorsal thalamus (MD; anteroposterior −1.34, ML 1.21, DV −2.99; pipette at an angle of 15°), in the ATN (anteroposterior −0.9, ML 1.6, DV −2.88; pipette at an angle of 15°), in the claustrum (CLA; anteroposterior 1.1, ML 2.9, DV −2.7), in the basolateral amygdala (BLA; anteroposterior 1.4, ML 3.1, DV −3.9) in the primary sensory cortex of the hind limp at two different points (S1HL; anteroposterior −0.3/−0.7, ML 1.45/1.5, DV −1.1/−1.1), in the ipsilateral ACC (iACC; anteroposterior 0.4, ML 0.3, and DV −1.7), and in the retrosplenial cortex (RSC; anteroposterior −2.9, ML 0.45, DV −1.1). In the left hemisphere, mice were injected in the contralateral ACC (cACC) at four different points (anteroposterior 1.1/0.8/0.5/0.2, ML 0.3 and DV 1.8/1.75/1.7/1.7). All coordinates for the DV axis were measured from the skull on, except for the thalamic injections where DV was zeroed at the sagittal suture at the respective anteroposterior point. At the end of the surgery, mice received a subcutaneous injection (in μg per gram of bodyweight) of 2 dexamethasone (Mepha Pharma) and 5 Caprofen-Rimadyl (Zoetis).

Confocal imaging and axon density analysis. Brain slices used for electrophysiological recordings were fixed in 4% PFA at 4°C overnight. After washing the slices with PBS (3× for 10 min), they were permeabilized in PBS containing 2% Triton X-100 for 1 h. Then slices were incubated with streptavidin-conjugated Alexa-488/Alexa-594/Alexa-405 (1:200; Invitrogen) in PBS containing 1% Triton X-100 depending on the axonal fluorescence tag. After washing with PBS (3× for 10 min), the processed slices were embedded in Mowiol on microscopy slides. Fluorescently labeled coronal brain slices were imaged using a confocal microscope (Leica Microsystems, SP8) equipped with a white-light laser and two GaAsP-detectors (HyD). Imaging was performed with a 20× objective (Leica Microsystems, HC PL APO, 20×, NA 0.75 IMM CORR CS2) from the rostral ACC. The region containing the labeled pyramidal neuron was imaged in the tile-scan mode from the midline to L6. Fluorescence profiles of axon density were determined with ImageJ using 6-10 slices per afferent input target. Intensity profiles were aligned to the midline, normalized to the peak fluorescence and averaged.

Data analysis. Data were analyzed using custom-written IGOR procedures. The program Prism (GraphPad) was used for statistical analysis, and data were tested with paired or unpaired Student's *t* test, or with one- or two-way ANOVA together with *post hoc* Tukey test or Holm–Sidak correction for multiple comparisons. Statistical significance was asserted for $p < 0.05$. Data are mean ± SEM. Coefficient of variation was calculated as $CV^{-2} = \mu^2/\sigma^2$ and variance-to-mean ratio as VMR = σ^2/μ, with μ being the mean amplitude of the postsynaptic potential and σ^2 its variance.

Chemicals. Chemicals were obtained from the following producers: D-(−)-2-amino-5-phosphonopentanoic acid (APV, 50 μM) and MPEP (10 μM) from Abcam; CNQX (10 μM) and KT-5823 (0.5 μM) from Tocris Bioscience; gabazine (1 μM), Ro 25-6981 maleate salt (0.5 μM), (S)-(+)-a-amino-4-carboxy-2-methylbenzeneacetic acid (LY-367385, 100 μM), S-nitroso-*N*-acetyl-DL-penicillamine (SNAP, 200 μM), 1H-[1,2,4]oxadiazolo[4,3-a]quinoxalin-1-one (ODQ, 10 μM), (+)-5-methyl-10,11-dihydro-5H-dibenzo[a,d]cyclohepten-5,10-imine maleate (MK801, 1 mM), and carboxy-PTIO potassium salt (cPTIO, 30 μM) from Sigma; and TTX from Alomone Labs.

Results

tLTD is absent in L5 pyramidal neurons in the ACC in animals with nerve injury

First, we confirmed that tLTD could be induced in L5 pyramidal neurons in the ACC of mice that had undergone sham surgery of the sciatic nerve. We established whole-cell recordings from pyramidal neurons and recorded EPSPs evoked by extracellular stimulation (0.1 Hz) at the border between L2/3 and L5 (Fig. 1*A*). tLTD was induced by pairing EPSPs with a preceding AP evoked by somatic current injection (AP-EPSP pairing, time interval $\Delta t = -25$ ms, 60 AP-EPSP pairings at 0.1 Hz). This protocol induced strong, long-lasting synaptic depression with an average reduction in EPSP amplitudes by a factor of 0.69 ± 0.13 ($n = 11$, $F_{(1,20)} = 5.45$, $p < 0.05$, two-way ANOVA) measured 20-40 min after pairing (Fig. 1*B*—*D*). In contrast, the same pairing protocol did not induce tLTD in slices from mice that had

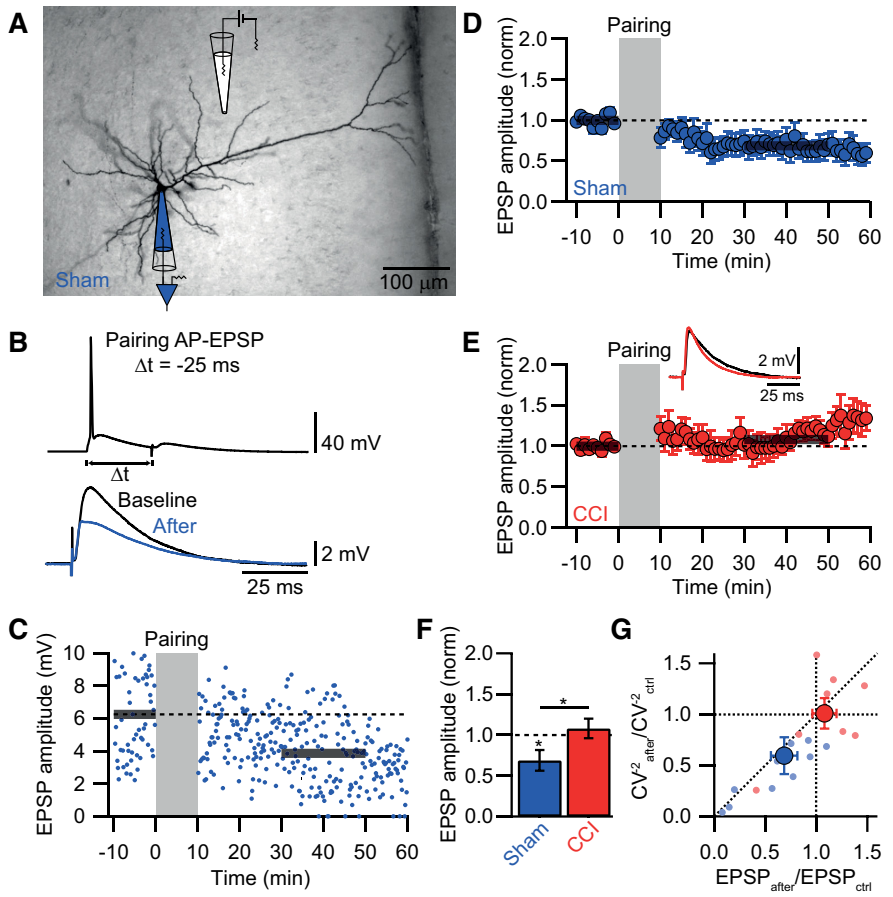

Figure 1. CCI impairs tLTD in the ACC. ***A***, Reconstruction of an L5 pyramidal neuron in the ACC, illustrating the recording configuration. Electrical stimulation was performed at the border to L2/3. ***B***, tLTD was induced by AP-EPSP pairing ($\Delta t = -25$ ms) repeated 60× at 0.1 Hz (top). Average EPSP recorded before (black) and 20-40 min after pairing (blue; bottom traces). ***C***, EPSP amplitudes plotted over time for an example tLTD experiment in a sham animal. Gray area represents pairing period. Bold gray lines indicate average EPSP amplitude before and 20-40 min after pairing. ***D***, Normalized and pooled EPSP amplitudes over time for sham animals. ***E***, Normalized and pooled EPSP amplitude over time for CCI animals shows lack of tLTD. Inset, Example EPSPs before and after pairing as indicated by bold gray lines. ***F***, Bar graph summary comparing the amount of tLTD in sham and CCI. A significant difference ($^*p < 0.05$) was found. ***G***, Analysis of the change in the CV^{-2} of EPSP amplitudes after pairing for sham (blue) and CCI (red). Small circles represent individual experiments. Large circles represent the mean ± SEM.

undergone CCI of the sciatic nerve 10-14 d before recording. The average EPSP amplitude remained unchanged by a factor of 1.08 ± 0.12 ($n = 8$, $F_{(1,14)} = 0.39$, $p = 0.54$, two-way ANOVA; Fig. 1*E*,*F*). This was significantly different compared with the change in EPSP amplitude in sham animals ($F_{(1,34)} = 4.64$, $p < 0.05$, two-way ANOVA). Plotting the change in CV^{-2} against the change in EPSP amplitude after pairing revealed a linear relationship between the two for sham experiments, indicating a presynaptic locus of tLTD. In contrast, the CCI condition showed on average no changes in CV^{-2} and EPSP amplitude (Fig. 1*G*). These results indicate that tLTD was impaired in L5 pyramidal neurons of the ACC after the development of nerve injury-induced neuropathic pain.

The tLTD phenotype has an early onset and is maintained after spontaneous recovery from mechanical hypersensitivity

Little is known about the progression of synaptic changes during the development of chronic pain as most studies focus on a single time point after the establishment of the sensitized state. Our experiments revealed that the loss of tLTD was present between 10 and 14 d after CCI surgery, a time span characterized by stable mechanical hypersensitivity (Fig. 2*A*). In order to elucidate the time course of the tLTD phenotype, we also measured the induction of tLTD already 2 d after sham or CCI surgery. At this time point, the sensitization had just been established in the CCI condition (Fig. 2*A*). As expected, sham animals showed significant tLTD (0.74 ± 0.09, $n = 10$, $p < 0.05$, two-sided paired Student's t test; Fig. 2*C*). In CCI animals, tLTD was already absent 2 d after surgery (1.11 ± 0.13, $n = 9$, $p = 0.61$, two-sided paired Student's t test; Fig. 2*D*, *G*). Thus, the block of tLTD after CCI surgery had a rapid onset at cortical synapses onto L5 pyramidal neurons in the ACC.

Investigating the more long-term effect of CCI for up to 35 d revealed spontaneous recovery from mechanical hypersensitivity in a subset of animals (Fig. 2*A*,*B*); ~50% of animals (10 of 21 CCI animals) had recovered 35 d after surgery, whereas the other half still showed a stable mechanical sensitization. Next, we tested the induction of tLTD in these two groups. tLTD was still absent in the hypersensitive group (1.2 ± 0.09, $n = 11$, $p = 0.08$, two-sided paired Student's t test), but interestingly also in the group that had recovered (1.11 ± 0.06, $n = 10$, $p = 0.08$, two-sided paired Student's t test; Fig. 2*F*,*G*). In contrast, sham animals showed significant tLTD at this time point (0.86 ± 0.05, $n = 12$, $p < 0.05$, two-sided paired Student's t test, Fig. 2*E*,*G*). Plotting the magnitude of tLTD over time for sham and CCI and comparing this with tLTD in naive animals (Fig. 2*H*) illustrated the rapid onset and persistence of the tLTD phenotype in the CCI condition, independent from the mechanical sensitivity state of the animal. The absolute time the animals had recovered from hypersensitivity had no influence on the absence of tLTD (Fig. 2*I*). Plotting tLTD magnitude against the time of full recovery yielded no correlation ($p_r = 0.11$), suggesting that tLTD did not return even in animals that had lost mechanical sensitization for some time already (average recovered time 7.6 ± 1.1 d; range 1-13 d). Thus, these results show that nerve injury can result in a long-lasting alteration in synaptic plasticity rules that last beyond the time of healing. This imprint of a previous painful experience might be caused by synaptic metaplasticity that permanently influences the signaling mechanism for tLTD in CCI.

Molecular signaling cascade for tLTD in L5 pyramidal neurons of the ACC

In order to identify the cellular signaling cascade for tLTD that was impaired in the CCI condition, we first elucidated the induction mechanism in slices from naive animals (Fig. 3). tLTD of a similar magnitude was obtained in this case (EPSP amplitude reduction by a factor of 0.71 ± 0.08, $n = 18$, $p < 0.05$, two-sided Student's t test). Furthermore, the change in CV^{-2} covaried with the change in EPSP amplitude, again suggesting a presynaptic

locus for the expression of tLTD (Fig. 3*H*). Presynaptic modifications in synaptic strength require retrograde signaling from the postsynaptic to the presynaptic site. Endocannabinoids are the retrograde messenger for the induction of tLTD at cortical synapses in the somatosensory and visual cortex (Sjostrom et al., 2003; Bender et al., 2006; Nevian and Sakmann, 2006). Blocking of endocannabinoid Type 1 receptors with the antagonist AM251 (5 μM) had no effect on the induction of tLTD. The average EPSP amplitude was reduced by a factor of 0.71 ± 0.12 ($n = 9$, $p < 0.05$, two-sided Student's t test), not significantly different from the EPSP amplitude in the absence of the drug ($p = 0.97$, one-way ANOVA). Another retrograde messenger that has been implicated in synaptic plasticity is NO. Bath application of the NO scavenger cPTIO (30 μM) blocked the induction of tLTD (1.05 ± 0.03, $n = 11$). The wash-in of SNAP (200 μM), a NO donor, for 10 min after baseline, while continuing synaptic stimulation resulted in a significant reduction in EPSP amplitude (0.60 ± 0.12, $n = 6$, $p < 0.05$, two-sided Student's t test). NO might exert its presynaptic action by activating guanylate cyclase, which increases the level of cGMP that then can bind to PKG, a known target to modulate presynaptic release. We blocked guanylate cyclase by ODQ (10 μM) and PKG by KT5823 (0.5 μM). Both antagonists prevented the induction of tLTD (ODQ: 0.97 ± 0.04, $n = 7$, $p = 0.94$, two-sided Student's t test; KT5823: 0.99 ± 0.03, $n = 8$, $p = 0.21$, two-sided Student's t test). These results suggest that NO is the retrograde messenger in tLTD at L5 pyramidal neuron synapses in the ACC.

The function of nNOS, the enzyme that catalyses NO production, is Ca^{2+}-dependent (Zhou and Zhu, 2009). Indeed, buffering Ca^{2+} to the physiological resting levels in L5 pyramidal neurons with a Ca^{2+} clamp solution containing BAPTA (Nabavi et al., 2013) during the AP-EPSP pairing blocked the induction of tLTD (0.96 ± 0.15, $n = 9$, $p = 0.95$, two-sided paired Student's t test; Fig. 4*A*). Next, we investigated which Ca^{2+} source might be involved in tLTD (Fig. 4*B*—*E*). Blocking mGluRs with a cocktail of LY-367385 (100 μM) and MPEP (10 μM) had no effect on tLTD (0.73 ± 0.07, $n = 16$, $p < 0.005$, two-sided paired Student's t test), suggesting that mGluR1 and mGluR5 are not involved. Bath application of the

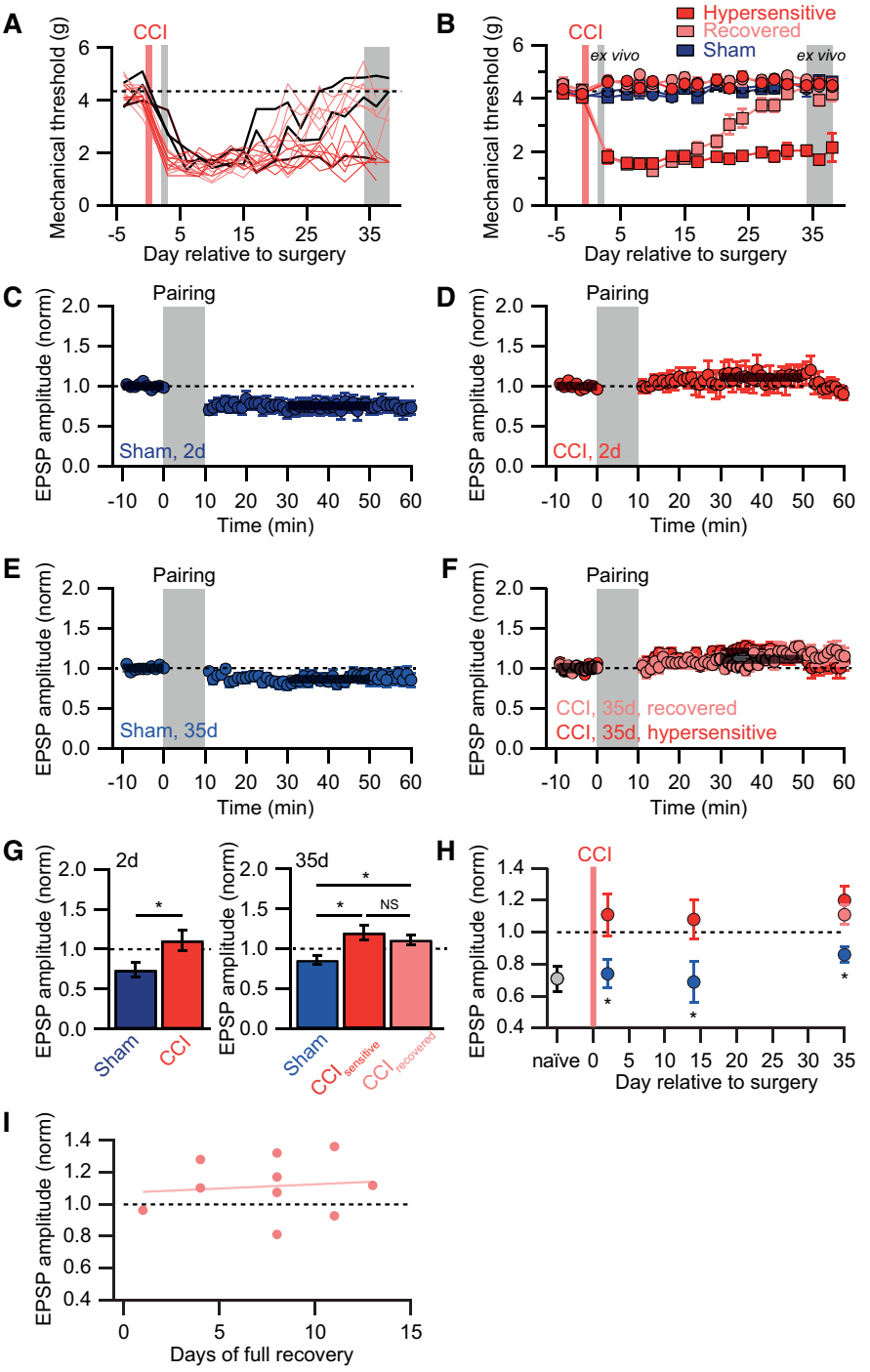

Figure 2. tLTD impairment shows early onset and is maintained after recovery from mechanical sensitization. ***A***, Time course of the mechanical threshold of the injured hindpaw for different animals. In all cases, CCI surgery (red shaded area) resulted in sensitization (i.e., decrease in mechanical threshold). After 35 d, a fraction of animals had recovered from mechanical hypersensitivity (light red), whereas others were still hypersensitive (dark red). Black traces represent three examples of no recovery, slow recovery, and early recovery. Gray shaded areas represent time periods in which brain slices were prepared for tLTD experiments. ***B***, Averaged time course of the mechanical threshold for animals that recovered (light red) or remained hypersensitive (dark red) for the left injured (squares) and right noninjured (circles) hindpaws. Sham animals did not show any change in mechanical threshold (blue). ***C***, ***D***, Normalized and pooled EPSP amplitudes over time for tLTD experiments performed 2 d after surgery for (***C***) sham and (***D***) CCI. ***E***, ***F***, Normalized and pooled EPSP amplitudes over time for tLTD experiments performed 35 d after surgery for (***E***) sham animals and (***F***) the two groups of recovered (light red) and still hypersensitive (dark red) animals after CCI. ***G***, Bar graph summary of the different conditions. ***H***, Time course of the tLTD for sham (blue) and CCI (red). tLTD in the naive condition (gray) is added as reference. ***I***, Plot of tLTD against the number of days of full recovery for individual animals. Solid line indicates a linear fit. Data are mean ± SEM. *$p < 0.05$.

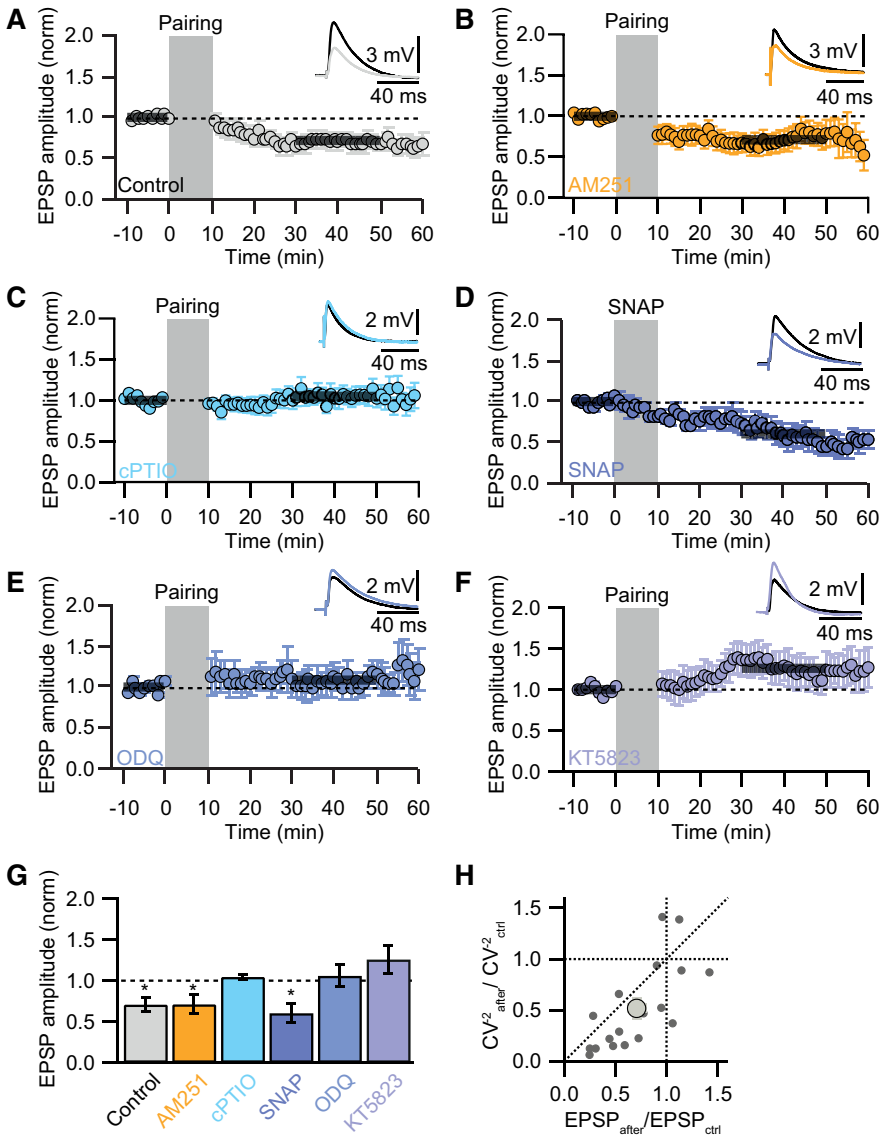

Figure 3. Noncanonical retrograde signaling in tLTD. ***A***, Normalized and pooled EPSP amplitudes over time for control experiments. Inset, Representative EPSP average during baseline (black) and after tLTD induction (gray). Bolt gray bars represent average EPSP amplitudes over the indicated time period. ***B–F***, Normalized and pooled EPSP amplitudes over time for different pharmacological manipulations. ***B***, In the presence of the endocannabinoid receptor type 1 antagonist AM251. ***C***, In the presence of the NO scavenger cPTIO. ***D***, Bath application of the NO donor SNAP. ***E***, In the presence of the guanylate cyclase inhibitor ODQ. ***F***, In the presence of the PKG blocker KT5823. ***G***, Bar graph summary of experiments shown in ***A–F***. ***H***, Analysis of the change in the CV^{-2} of EPSP amplitudes after pairing for control tLTD experiments in naive animals. Small circles represent individual experiments. Large circle represents the mean. Data are mean ± SEM. $^*p < 0.05$.

NMDAR antagonist APV (50 μm) completely abolished tLTD (1.27 ± 0.12, $n = 9$, $p = 0.05$, two-sided Student's t test). Infusion of the NMDAR blocker MK801 (1 mM) into the postsynaptic pyramidal neuron also blocked tLTD (1.01 ± 0.09, $n = 10$, $p = 0.94$, two-sided paired Student's t test), suggesting that postsynaptic NMDARs are involved in this form of plasticity. The GluN2B subtype-specific blocker Ro 25-6981 (0.5 μM) was sufficient to abolish tLTD (0.98 ± 0.02, $n = 9$, $p = 0.27$, two-sided paired Student's t test). These results suggest that elevations of postsynaptic Ca^{2+} through GluN2B-containing NMDARs are essential for the induction of tLTD (Fig. 4*F*).

Loss of GluN2B-containing NMDARs in neuropathic pain

After the identification of the key mechanisms in the induction of tLTD, we wondered which element of the signaling cascade was disrupted in the neuropathic pain condition. First, we tested the presynaptic signaling cascade activated by NO (Fig. 5*A*). Bath application of the NO donor SNAP resulted in a decrease in EPSP amplitude both in sham and CCI animals (sham: 0.66 ± 0.13, $n = 7$, $p = 0.03$, two-sided Student's t test; CCI: 0.57 ± 0.11, $n = 6$, $p = 0.02$, two-sided Student's t test), suggesting that the presynaptic expression mechanism was still intact in CCI. Nevertheless, the time course of SNAP-induced depression was different in the two conditions. Fitting a sigmoidal function to the evolution of the EPSP amplitude in the presence of SNAP yielded a significant difference in the half-time to depression in sham and CCI (sham: 25.8 ± 4.2 min, $n = 7$; CCI: 8.6 ± 2.6 min, $n = 6$; $p < 0.01$, one-way ANOVA). The time course of SNAP-induced depression was comparable between sham and the naive condition (naive: 28.7 ± 6.7 min, $n = 6$; Fig. 3*D*).

To investigate whether neuropathic pain causes changes at the postsynaptic site, we studied AMPAR and NMDAR functioning. In a first step, we measured the ratio of currents mediated by these two receptors, and we found that the NMDA-to-AMPA ratio was significantly different between sham and CCI ($p < 0.02$, one-way ANOVA) with a higher ratio in the CCI condition (sham: 0.23 ± 0.03, $n = 9$; CCI: 0.35 ± 0.04, $n = 13$; Fig. 5*B*). In order to test for an involvement of postsynaptic modifications of AMPARs, we compared the I–V relationship of AMPAR-mediated currents in sham and CCI (Fig. 5*C*). Both I–V curves showed a linear relationship and were identical, ruling out a modification of postsynaptic AMPARs in the neuropathic pain condition. Nonstationary fluctuation analysis of AMPAR currents in sham and CCI furthermore revealed that neither channel number nor single-channel conductance was different in the two conditions (Fig. 5*D*). Thus, these findings suggested that postsynaptic AMPA functioning was unchanged but that the NMDAR component was modified in the condition of neuropathic pain.

We hypothesized that the loss of tLTD in CCI might be because of a modification in GluN2B-containing NMDARs as they were essential for the synaptic depression. We measured isolated NMDAR currents and bath-applied the GluN2B-selective antagonist Ro 25-6981, while continuing synaptic stimulation (Fig. 5*E*). In the presence of Ro 25-6981, the NMDA-mediated current was reduced and a fraction of 0.78 ± 0.04 ($n = 7$) remained in sham operated animals. In contrast, Ro 25-6981 had no influence in the CCI condition (0.97 ± 0.06, $n = 8$). The effect of the GluN2B-block was significantly different in the two conditions ($p < 0.05$, one-way ANOVA). Subsequent bath application of APV abolished all

currents and confirmed that we only had measured NMDAR-mediated currents. In summary, we identified a switch in the NMDA subunit composition, excluding GluN2B-containing NMDARs, as the cellular mechanism that can explain the loss of tLTD in neuropathic pain.

Afferent pathway-specific loss of GluN2B-containing receptors at synapses onto L5 pyramidal neurons in the ACC

The ACC receives afferent input from many brain areas (Fillinger et al., 2017), and it is likely that a number of them directly contact L5 pyramidal neurons. We tested functional connectivity by transducing channel rhodopsin 2 (ChR2) with a viral vector in the most prominent projection areas to the ACC that are involved in transmitting nociceptive information (Fig. 6*A*). cACC, CLA, RSC, ATN, MD, and BLA had high connection probability to L5 pyramidal neurons in the ACC ranging from 70% to 100%, although the axonal projection pattern from the different brain areas differed considerably (Fig. 6*B—D*). Only the projection from the hindlimb region of the somatosensory cortex was not directly connected to L5 pyramidal neurons in the ACC.

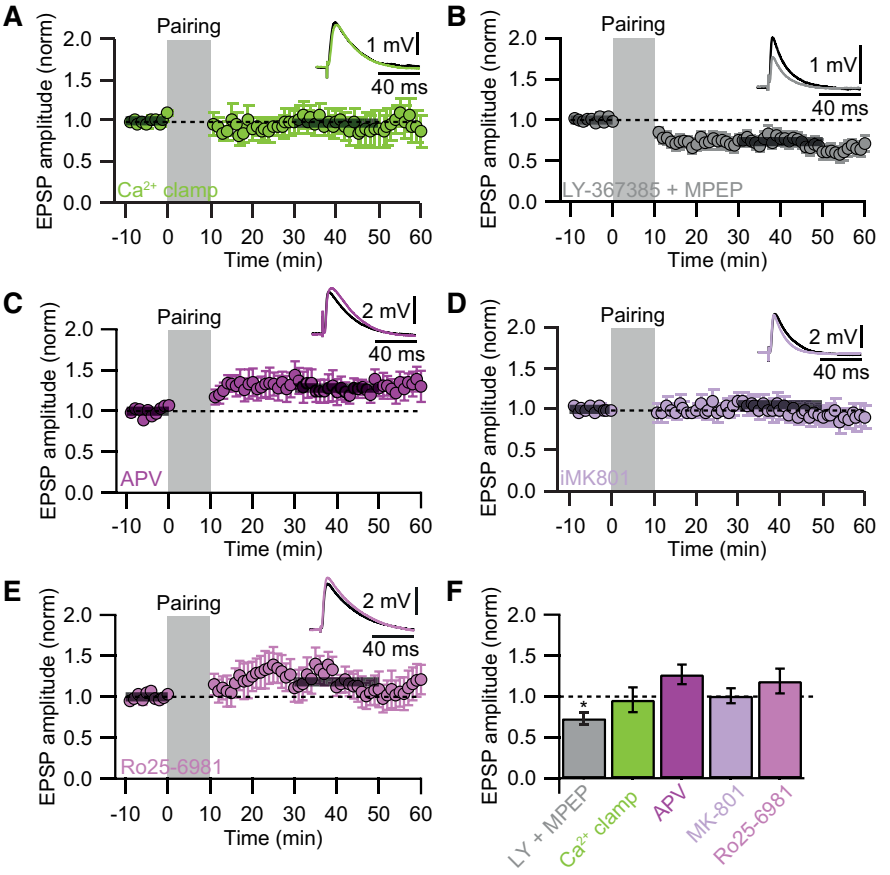

Figure 4. LTD induction requires Ca^{2+} signaling and GluN2B activity but not mGluRs. ***A–E***, Normalized and pooled EPSP amplitudes over time for different pharmacological manipulations. Inset, Representative averaged EPSP during baseline (black) and after tLTD induction (color). Bolt gray bars represent average EPSP amplitudes over the indicated time period. ***A***, Buffering of intracellular Ca^{2+} with a Ca^{2+} clamp solution. ***B***, In the presence of the mGluR blockers LY367385 and MPEP. ***C***, In the presence of APV. ***D***, In the presence of intracellularly applied MK801. ***E***, In the presence of the GluN2B blocker Ro 25-6981. ***F***, Bar graph summary of experiments shown in ***A–E***. Data are mean ± SEM. *$p < 0.05$.

In order to answer the question of whether the synaptic phenotype was global or attributable to a specific pathway, we determined the contribution of the GluN2B subunit for the different afferent inputs in sham and CCI. We also included projections within the ACC of the ipsilateral hemisphere (iACC) by expressing ChR2 in more posterior parts of the ACC. We observed that stimulation of projections from the cACC, iACC, RSC, and ATN evoked considerable NMDAR currents measured at a holding potential of 40 mV (cACC: 271.8 ± 82.4 pA; iACC: 402.6 ± 54.4 pA; RSC: 130.5 ± 22.5 pA; ATN: 281.8 ± 57.9 pA), while activation of projections from the CLA, MD, and BLA generated only very small currents (CLA: 12.7 ± 4.3 pA; MD: 9.6 ± 2.9 pA; BLA: 39.0 ± 8.1 pA; Fig. 6*E*). Therefore, the GluN2B component was determined by the effect of Ro 25-6981 on the isolated NMDA current amplitude only for the most prominent inputs (Fig. 6*F*). The inputs from the contralateral and iACC as well as the inputs from the RSC showed the same reduction in the NMDA current amplitude after bath application of Ro 25-6981 in sham and CCI, suggesting that they had the same GluN2B component in both conditions (relative drug effect; iACC, sham, 0.84 ± 0.04; CCI, 0.80 ± 0.02, $p = 0.53$; cACC, sham, 0.78 ± 0.04, CCI, 0.78 ± 0.04, $p = 0.89$; RSC, sham, 0.81 ± 0.08, CCI, 0.77 ± 0.04, $p = 0.61$). In contrast, NMDA currents evoked by stimulation of afferents from the ATN were not sensitive to Ro 25-6981 in CCI animals anymore (sham, 0.81 ± 0.05, CCI, 0.93 ± 0.02, $p < 0.05$), indicating that they had lost their GluN2B component. This switch in NMDA subunit composition should have an impact on the kinetics of the NMDA current evoked by ATN stimulation (Paoletti et al., 2013). Analysis of the NMDA currents in the sham condition revealed different kinetics for the ATN inputs compared with the cortical inputs. NMDA currents at ATN synapses had an apparent slower rise time (cACC 4.6 ± 0.1 ms; iACC 5.0 ± 0.3 ms; RSC 5.1 ± 0.2 ms; ATN 8.5 ± 0.4 ms), a more rapid τ_{fast} (cACC 41.8 ± 1.8 ms; iACC 40.8 ± 2.2 ms; RSC 33.2 ± 2.0 ms; ATN 28.9 ± 2.1 ms), and a slower τ_{slow} (cACC 199.6 ± 12.2 ms; iACC 197.9 ± 8.8 ms; RSC 189.0 ± 19.3 ms; ATN 231.7 ± 16.2 ms; Fig. 6*G*,*I*). These kinetic parameters were not altered in CCI at the cortical inputs (rise time: cACC 4.9 ± 0.2 ms; iACC 4.8 ± 0.1 ms; RSC 5.4 ± 0.2 ms; τ_{fast}: cACC 36.9 ± 1.3 ms; iACC 45.4 ± 2.4 ms; RSC 35.6 ± 1.6 ms; τ_{slow}: cACC 180.5 ± 9.6 ms; iACC 208.6 ± 5.4 ms; RSC 212.2 ± 21.5 ms; Fig. 6*H*). At the ATN synapse, rise time (8.3 ± 0.2 ms) and τ_{fast} (29.3 ± 1.2 ms) were also not changed, whereas τ_{slow} (190.9 ± 7.6 ms) was significantly faster in CCI ($p < 0.05$, one-way ANOVA; Fig. 6*I*). This change in τ_{slow} is consistent with a loss of the GluN2B subunit as GluN2B lacking NMDARs have a faster decay (Vicini et al., 1998; Erreger et al., 2005). Thus, these results suggest that the synaptic phenotype described above was pathway specific for connections from the ATN and not a global phenomenon.

Therefore, we investigated whether the postsynaptic lack of GluN2B at the ATN-to-L5 pyramidal neuron connection in the ACC in the CCI condition resulted in the loss of tLTD at this specific synapse (Fig. 7). Pairing of optogenetically evoked EPSPs

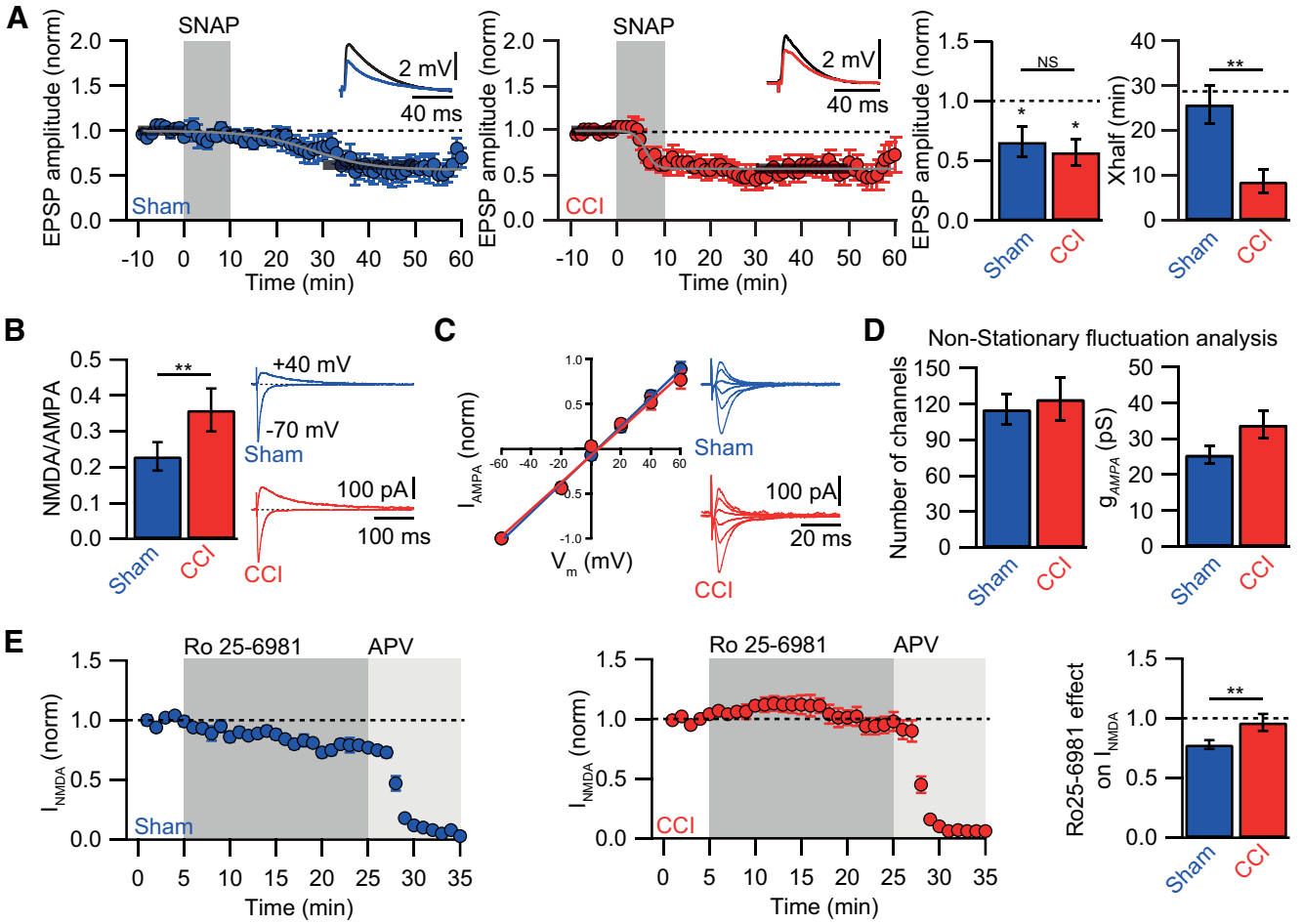

Figure 5. Mechanism of tLTD pathology in CCI. ***A***, Normalized and pooled EPSP amplitudes over time for sham (blue) and CCI (red). Shaded area represents the time of bath application of the NO donor SNAP. Inset, Representative averaged EPSPs during baseline (black) and after tLTD induction (color). Bolt gray bars represent average EPSP amplitudes over the indicated time period. Solid gray lines indicate sigmoidal fits to the EPSP amplitudes over time. Middle, Bar graph summary of normalized and averaged EPSP amplitudes after bath application of SNAP. Right, bar graph summary of the averaged sigmoidal half-points to depression (Xhalf) for the SNAP experiments. Dashed line indicates Xhalf for the naive condition. ***B***, Bar graph summary of the NMDA-to-AMPA-ratio in sham and CCI. Right, Representative current traces for sham and CCI at different holding potentials. ***C***, I–V curve of isolated AMPAR currents showing a linear relationship for sham (blue) and CCI (red). Right, Representative current traces for sham and CCI. ***D***, Estimation of the number of channels (left bar graph) and single-channel conductance (g_{AMPA}; right bar graph) via peak-scaled nonstationary fluctuation analysis indicated that channel properties of AMPARs were the same in sham (blue) and CCI (red). ***E***, Normalized and pooled NMDA-EPSC amplitudes over time for sham (blue) and CCI (red). Dark shaded area represents the time of bath application of the GluN2B blocker Ro 25-6981. Light shaded area represents bath application of APV. Right, Bar graph summary of the effect of Ro 25-6981 on NMDA-EPSC amplitudes showing that, in the CCI condition, the block of GluN2B-containing NMDARs had no effect. Data are mean ± SEM. *$p < 0.05$. **$p < 0.01$.

from the ATN with a preceding AP in L5 pyramidal neurons in the ACC (AP-EPSP pairing, time interval $\Delta t = -25$ ms, 60 AP-EPSP pairings at 0.1 Hz; Fig. 7*B*) induced tLTD in sham animals with an average reduction in EPSP amplitude by a factor of 0.79 ± 0.06 ($n = 8$, $p < 0.01$, two-sided paired Student's t test; Fig. 7*C*). In the CCI condition, tLTD was indeed abolished (1.07 ± 0.07, $n = 6$, $p = 0.31$, two-sided paired Student's t test; Fig. 7*D*). This was significantly different compared with the change in EPSP amplitude in sham animals ($p < 0.01$, one-way ANOVA; Fig. 7*H*). CV analysis confirmed the presynaptic origin of tLTD in sham and a loss of presynaptic modification in CCI (Fig. 7*G*).

To assess the specificity of the tLTD phenotype, we tested with optogenetic stimulation whether other pathways exhibited an impairment of tLTD in CCI as well. Pairing afferent inputs from the cACC with a preceding AP at $\Delta t = -25$ ms resulted in tLTD in sham (0.69 ± 0.07, $n = 9$, $p < 0.01$, one-way ANOVA; Fig. 7*E*) and also in CCI animals (0.71 ± 0.06, $n = 9$, $p < 0.01$, one-way ANOVA; Fig. 7*F*). When testing tLTD at RSC-to-ACC synapses, we found that tLTD was absent already in naive animals (1.08 ± 0.11, $n = 8$, $p = 0.97$, one-way ANOVA; Fig. 7*J*, *L*), in contrast to naive inputs from the cACC (0.81 ± 0.05, $n = 25$, $p < 0.01$, one-way ANOVA; Fig. 7*I*) and ATN (0.76 ± 0.05, $n = 8$, $p < 0.01$, one-way ANOVA; Fig. 7*K*). These results suggest that the plasticity rules at different inputs onto L5 pyramidal neurons in the ACC are already different in the naive condition. But importantly, tLTD is differentially impaired in CCI depending on the presynaptic afferent inputs. In summary, tLTD is lost in neuropathic pain in a pathway-specific manner at the ATN-to-ACC L5 pyramidal synapse by a synapse-specific switch in NMDAR composition.

As a consequence, this specific loss of tLTD resulted on average in stronger synapses at the ATN-to-ACC connection in CCI compared with sham (sham: 4.45 ± 0.59 mV, $n = 10$; CCI: 7.81 ± 0.52 mV, $n = 10$; $p < 0.001$, one-way ANOVA corrected with Holm–Sidak; Fig. 8*A*,*B*). EPSPs in naive animals were similar to sham (naive: 5.30 ± 0.95; $p = 0.22$, one-way ANOVA corrected with Holm–Sidak), suggesting that we were indeed able to derive differences in synaptic strength from afferent ChR2 stimulation in

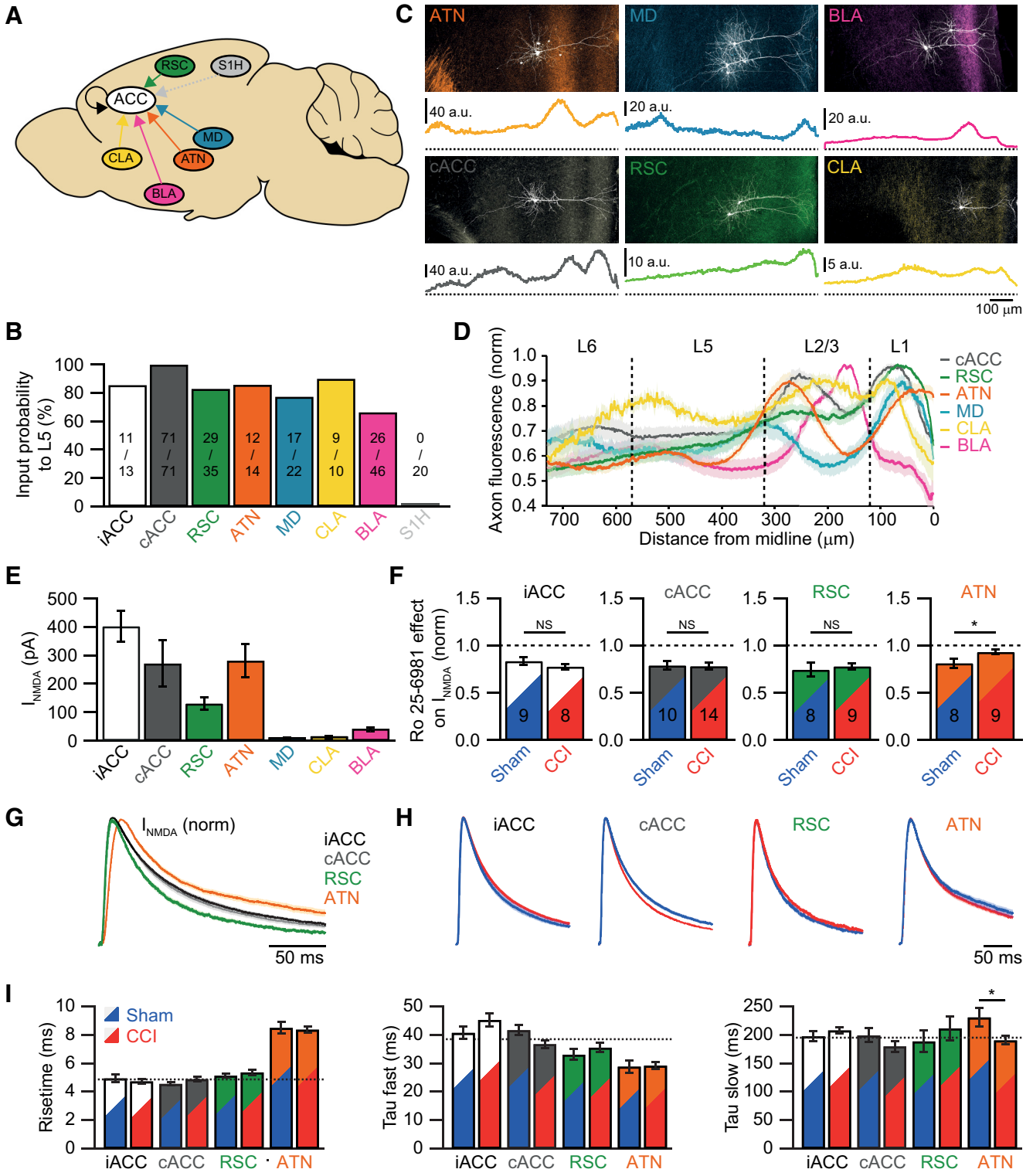

Figure 6. Pathway-specific exclusion of GluN 2B receptors in CCI. ***A***, Sketch illustrating the afferent input pathways to the ACC that were tested with ChR-2. ACC, RSC, primary somatosensory cortex of the hindlimb (S1H), CLA, BLA, MD, and ATN. ***B***, Summary bar graph of input probability to L5 pyramidal neurons in the ACC from the different brain areas. The numbers indicate the number of connections found and total number of trials. All areas, except S1H, had a high input probability. ***C***, Confocal images of the fluorescently labeled afferent axons from the different projections to the ACC. White represents the corresponding L5 pyramidal neurons. Below each image, intensity profile of axon fluorescence. ***D***, Normalized and averaged intensity profiles of axon fluorescence for the different afferent input pathways tested. Each input had a distinct innervation pattern in the ACC. Solid lines indicate mean intensity. Shaded areas represent SEM. ***E***, Bar graph summary of the total light-evoked, NMDAR-mediated currents (I_{NMDA}) of the different projections to the ACC. ***F***, Bar graph summary of the effect of the GluN 2B antagonist Ro 25-6981 on NMDAR-mediated EPSCs in sham and CCI conditions for the different afferent projections. Only the projection from the ATN was insensitive to Ro 25-6981 in CCI. ***G***, Averaged and normalized NMDAR-mediated EPSCs for the different afferent inputs measured at a holding potential of 40 mV in the sham condition. Note the slower rise and decay times for inputs from the ATN. ***H***, Averaged NMDAR-mediated EPSCs for the different afferent inputs comparing sham (blue) and CCI (red). ***I***, Bar graph summary of the kinetic parameters of the NMDAR-mediated EPSCs for the different afferent inputs in sham and CCI. Dashed lines indicate the average of the corresponding kinetic parameter from the cortical inputs (iACC, cACC, and RSC) in the sham condition. Data and NMDAR-mediated EPSCs are presented as mean ± SEM. *$p < 0.05$.

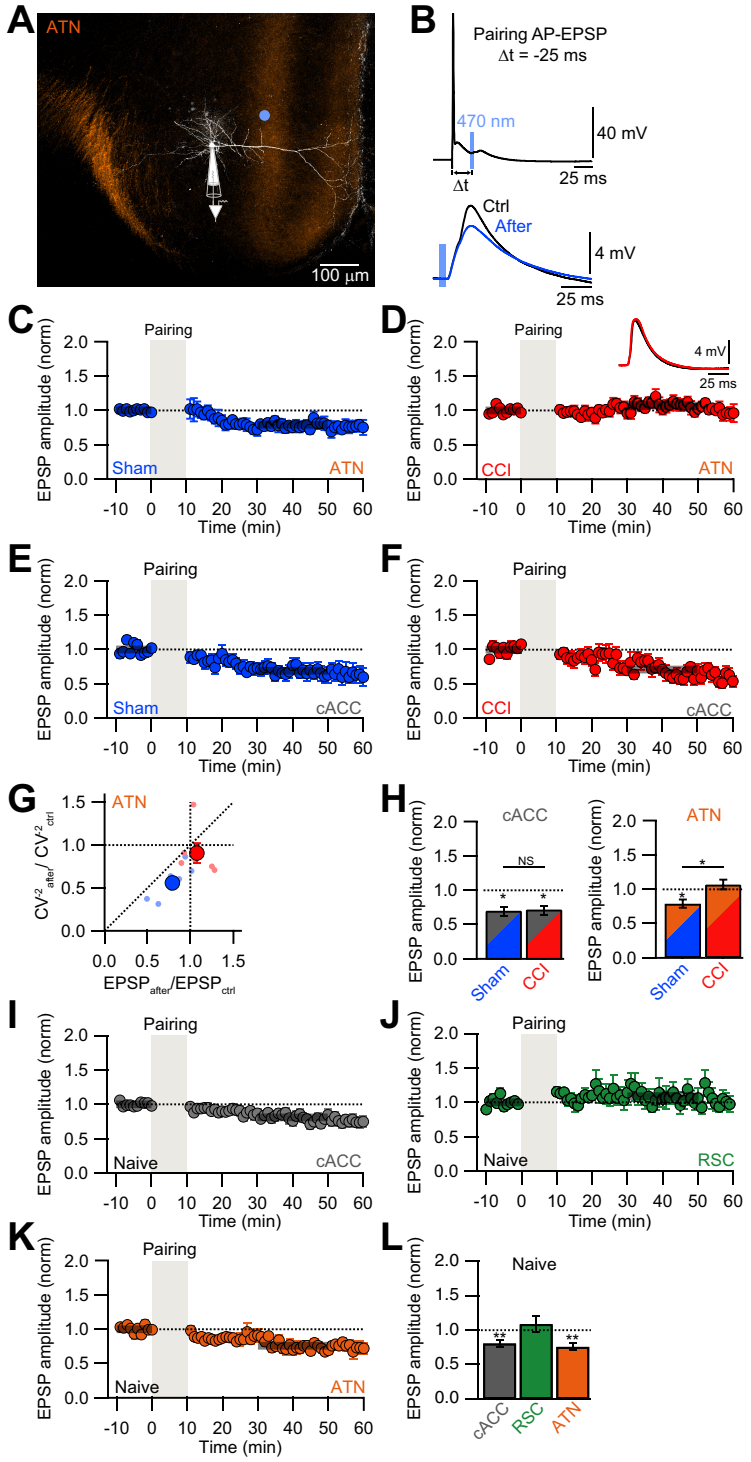

Figure 7. tLTD is specifically abolished at ATN-to-ACC synapses. ***A***, Confocal image of the fluorescently labeled afferent axons (orange) projecting from the ATN to the ACC. The corresponding L5 pyramidal neuron is shown in white, illustrating the recording configuration. Blue dot indicates site of light stimulation in L2/3. ***B***, Recordings from the cell shown in ***A***. tLTD pairing protocol (AP-EPSP, $\Delta t = -25$ ms; top). Blue bar represents time of light stimulation ($\lambda = 470$ nm, 5 ms). Average EPSP recorded before (black) and 20-40 min after pairing (blue; bottom traces). ***C***, ***D***, Normalized and pooled EPSP amplitudes over time for tLTD induction in ChR2-activated ATN-to-ACC connections in sham (***C***) and CCI (***D***). Bolt gray bars represent average EPSP amplitudes over the indicated time period. Inset, Representative average EPSP during baseline (black) and after tLTD induction (red). ***E***, ***F***, Normalized and pooled EPSP amplitudes over time for tLTD induction in ChR2-activated connections from cACC in sham (***E***) and CCI (***F***). Bolt gray bars represent average EPSP amplitudes over the indicated time period. ***G***, Analysis of the change in the CV^{-2} of EPSP amplitudes after pairing for sham (blue) and CCI (red) for ATN-to-ACC connections. Large circles represent the mean ± SEM. Small circles represent individual experiments. ***H***, Bar graph summaries comparing the amount of tLTD in sham and CCI for cACC (left) and ATN (right). ***I–K***, Normalized and pooled EPSP amplitudes over time for tLTD induction in ChR2-activated connections in naive animals from the cACC (***I***), RSC (***J***), and ATN (***K***). Bolt gray bars represent average EPSP amplitudes over the indicated time period. ***L***, Bar graph summary of the amount of tLTD in naive animals from different afferent inputs. Data are mean ± SEM. $^*p < 0.05$. $^{**}p < 0.01$.

the sham and CCI condition. Analysis of the EPSP fluctuations yielding the CV^{-2} and the VMR suggested that the increase in synaptic strength at the ATN-to-ACC synapse in CCI could be explained partly by a presynaptic alteration in release probability (van Huijstee and Kessels, 2020). CV^{-2} was significantly larger in CCI compared with sham (sham: 19.59 ± 3.69, $n = 10$; CCI: 43.98 ± 2.96, $n = 10$; $p < 0.001$, one-way ANOVA corrected with Holm–Sidak), whereas VMR was significantly smaller in CCI compared with sham (sham: 0.26 ± 0.03, $n = 10$; CCI: 0.18 ± 0.01, $n = 10$; $p < 0.05$, one-way ANOVA corrected with Holm–Sidak; Fig. 8*A*,*B*). According to the quantal model of synaptic transmission, this is consistent with an increase in release probability, but not with a change in the number of release sites or change in quantal size (van Huijstee and Kessels, 2020). Importantly, there were no such differences in CV^{-2} and VMR between the sham and naive condition ($p = 0.40$ and $p = 0.25$, respectively). Nevertheless, we additionally found a change in the rectification index of AMPA-EPSCs measured at −70 and 40 mV, respectively, between sham and CCI (sham, 1.41 ± 0.10, $n = 17$; CCI, 2.13 ± 0.28, $n = 18$; $p < 0.05$, one-way ANOVA; Fig. 8*D*,*E*), suggesting an increase in the AMPAR subunit GluA1 (Chen et al., 2014a). This could indicate that CCI induced LTP (Chen et al., 2014b) at the ATN-to-ACC synapse and concurrently impaired tLTD. In contrast, at the input from the cACC, no differences in average EPSP amplitude, CV^{-2}, and VMR were found between sham and CCI (Fig. 8*A*,*C*). This was consistent with the maintenance of tLTD at this synapse and confirmed that neuropathic pain resulted in a pathway-specific modification of the synaptic plasticity rules.

Discussion

Neuronal plasticity is a key mechanism for the chronification of pain (Kuner, 2010) and synaptic plasticity, the most prominent form of neuronal plasticity, that is instrumental for learning and memory, is also affected in chronic pain conditions. Thus, the concept of a "pain memory" as a persistent sensory memory of pain has emerged. It is well established that the aberrant neuronal activity in the pain processing system, caused by peripheral nerve damage or inflammation, leads to the engagement of synaptic plasticity mechanisms that enhance nociceptive information

transfer by LTP (Woolf, 1983; Woolf and Salter, 2000). Furthermore, LTP at specific synapses in the cortex might explain some of the comorbid symptoms of chronic pain, such as anxiety and depression (Koga et al., 2015). However, how this increase in synaptic strength, and therefore its contribution to the sensitization of the nociceptive system, is maintained is still elusive. The chronic pain state might be sustained by continuous induction of LTP or by postsynaptic signaling molecules that are important for the maintenance of LTP (Bliss et al., 2016). Here, the atypical protein kinase C isoform PKMzeta has been shown to stabilize LTP and chronic pain behaviors in mice (Li et al., 2010). Furthermore, molecules that have been shown to be involved in memory storage, such as CamKII, or nuclear signaling via CREB might also be involved in the development of chronic pain. Additionally, changes in glutamate receptor composition, such as increased GluN 2B or GluA 1 expression, can lead to metaplasticity that lowers the threshold for LTP induction (Bliss et al., 2016). The opposite mechanism to LTP, LTD is equally important for the formation of a memory. LTD enhances signal-to-noise after learning by reducing the influence of unrelated information, and it can depotentiate synapses to promote forgetting (Tsumoto, 1993). There are only a few reports that have shown an influence of chronic pain on LTD in the cortex so far (Liu and Zhuo, 2014). The development and maintenance of bone cancer pain are associated with a functional loss of LTD in L2/3 pyramidal neurons of the ACC (Chiou et al., 2012). Single-digit amputation (Wei et al., 1999) and mice with tail amputation (Kang et al., 2012), models that mimic phantom limb pain, also cause an impairment of LTD induced by low-frequency stimulation in the ACC.

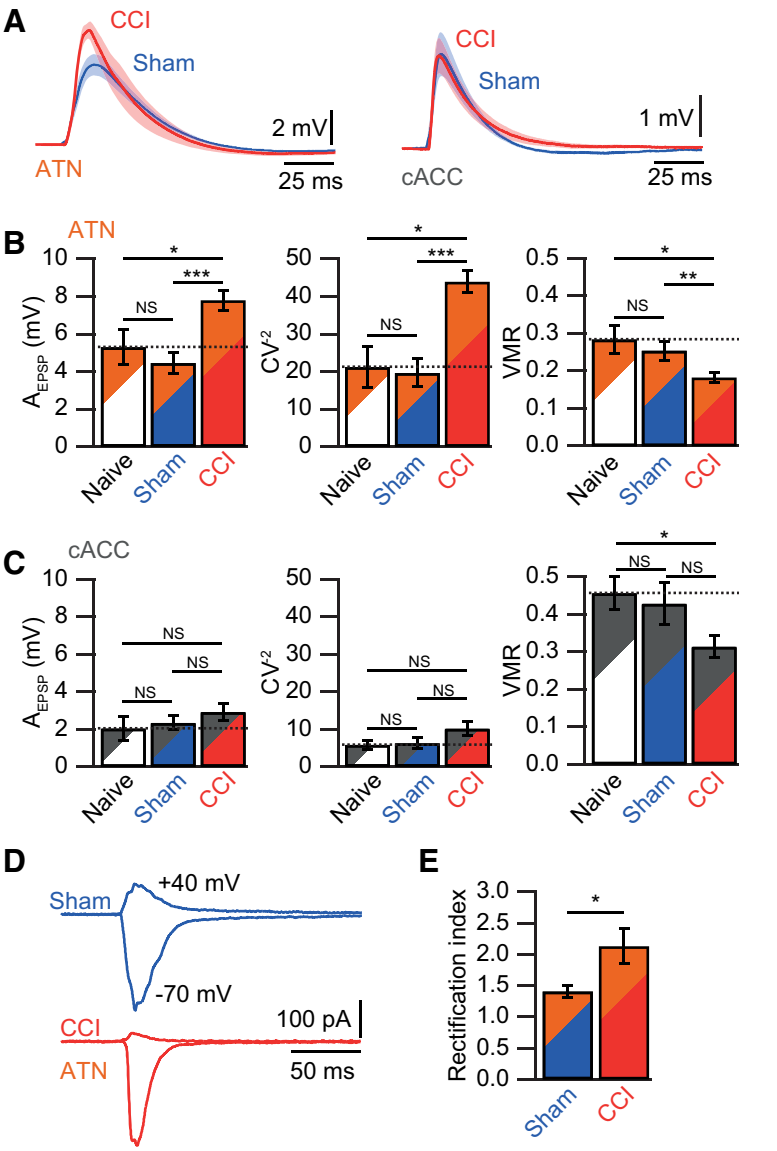

Figure 8. ATN-to-ACC synapses are potentiated in CCI. ***A***, Average EPSPs from ATN (left) and cACC (right) inputs of sham (blue) or CCI (red) animals. Shaded areas represent ± SEM. ***B***, Bar graph summary of EPSP amplitude (left), CV^{-2} (middle), and VMR (right) for naive, sham, and CCI for inputs from the ATN. ***C***, Bar graph summary of the same parameters for inputs from the cACC. ***D***, Example AMPA-EPSCs recorded at −70 mV and 40 mV from sham (blue) and CCI (red) at ATN synapses. ***E***, Bar graph summary of the rectification index for AMPA-EPSCs for sham and CCI at ATN synapses. Data are mean ± SEM. $*p < 0.05$. $**p < 0.01$. $***p < 0.001$.

We studied tLTD at synapses onto layer 5 pyramidal neurons in the ACC, a plausible mechanism for synaptic modifications in brain areas in which spiking activity is sparse (Barth and Poulet, 2012) and information is coded in the relative timing between presynaptic and postsynaptic activity. We found that this form of synaptic plasticity was impaired in neuropathic pain. The tLTD phenotype had a rapid onset and was already present 2 d after CCI, suggesting that the nerve injury impacts the whole pain processing system, including cortical areas immediately. These findings are consistent with the previous reports on a loss of LTD in the ACC in different pain models (Wei et al., 1999; Chiou et al., 2012; Kang et al., 2012). The tLTD phenotype persisted during the time of increased sensitivity to mechanical stimulation of the injured hindpaw, but strikingly also in animals that had spontaneously recovered from mechanical allodynia (Del Rey et al., 2011). Thus, the loss of tLTD was not correlated to the sensitivity state of the animal but might have relevance for the emotional processing of pain. Furthermore, this is the first report that a cortical synaptic plasticity phenotype persists after the time of healing from persistent pain, suggesting that a painful insult of the nervous system can leave a permanent trace manifested in this case as a change in synaptic plasticity rules. This metaplasticity might have important implications for future painful events as it might contribute to a facilitated relapse into the persistent pain state. Nevertheless, we cannot rule out that beyond 2 weeks after recovery tLTD might return, although we could not find any correlation between the time the animal had recovered and the magnitude of tLTD.

One major finding of our study is that the loss in tLTD was pathway-specific for inputs from the ATN onto L5 pyramidal neurons in the ACC. Thus, only specific inputs into the ACC are impacted by an increased nociceptive drive because of the peripheral nerve injury, suggesting that the plasticity is determined by the presynaptic drive and that the activity of the postsynaptic pyramidal neuron does not lead to a global modulation of synaptic strength. It is well established that the presynaptic and postsynaptic partners influence the rules of plasticity and synaptic

properties to a large extent (Reyes et al., 1998). This seems also to be true for synaptic modifications in the chronification of pain. Therefore, the synapse-specific rules for plasticity have to be taken into account when considering pharmacological strategies that are based on manipulating synaptic strength to treat chronic pain.

The cellular mechanism of tLTD at excitatory synapses onto L5 pyramidal neurons in the ACC of naive animals depends on postsynaptic calcium influx through GluN2B-containing NMDARs, which triggers the synthesis of the retrograde signaling molecule NO. NO binds to guanylate cyclase, resulting in an increase in cGMP and the activation of PKG, which downregulates presynaptic transmitter release. This is a novel mechanism for the induction of tLTD. So far, only 2-AG, an endocannabinoid, has been suggested to act as the retrograde messenger in tLTD at cortical synapses. Mechanistically, coincident activation of mGluRs and voltage-gated Ca^{2+} channels leads to activation of PLC, resulting in the generation and release of 2-AG from the postsynaptic compartment (Sjostrom et al., 2001; Bender et al., 2006; Nevian and Sakmann, 2006). 2-AG activates astrocytes that release glutamate onto presynaptic NMDARs (Min and Nevian, 2012; Neubauer et al., 2022), which are essential in the signaling cascade to downregulate release probability involving calcineurin (Rodriguez-Moreno et al., 2013). In contrast, we identified NO as the retrograde messenger, suggesting that tLTD can be implemented differentially at specific synapses. NO is implicated in synaptic plasticity at many different synapses for the induction of both LTD and LTP at excitatory synapses and also inhibitory synapses (Hardingham et al., 2013; Sieber et al., 2013; Lourenco et al., 2014).

The pathologic change that leads to a malfunction of tLTD in chronic pain specifically in the projections from ATN to ACC is caused by an exclusion of GluN2B-containing NMDAR from the postsynaptic site. This subunit is involved in different forms of synaptic plasticity because of the specific channel kinetics and intracellular binding partners (Paoletti et al., 2013). Particularly, GluN2B has been shown to couple to neuronal nNOS and that microdomain calcium signaling in this complex results in efficient synthesis of NO (Garthwaite, 2008). We suggest therefore that tLTD is impaired in the chronic pain conditions because GluN2B-containing NMDARs are excluded from the postsynaptic site reducing the functional coupling of nNOS (Park et al., 2020). As a consequence, the calcium-dependent production of NO is impaired. Additionally, GluN2B-containing NMDARs channel flux more calcium per unit of current than other subtypes (Sobczyk et al., 2005; Yashiro and Philpot, 2008). Thus, the substitution with GluN2A-containing NMDARs might also lead to a reduction in calcium influx, which additionally impairs nNOS function. Interestingly, although the wash-in of the NO-donor SNAP resulted in an equal amount of LTD in sham and CCI, the time course of this depression was different. SNAP-induced LTD developed more rapidly in CCI as compared with sham and the naive condition. This suggests that the presynaptic machinery translating a rise in NO in synaptic depression is not only intact in chronic pain animals, but it is also more sensitive. This difference could be the consequence of the tonic activation of the presynaptic signaling cascade of guanylate cyclace-cGMP-PKG when NO is released occasionally in the natural condition, whereas the lack of NO in CCI might render the system in a different, more sensitive state (e.g., the phosphorylation state of some targets of PKG might be different since the balance is shifted to phosphatases). When in this condition NO is supplied artificially, the whole system reacts faster.

Our finding that the metaplasticity switch preventing tLTD is based on the exclusion of GluN2B-containing NMDARs from the ATN-to-ACC synapse is important in light of an opposite regulation of this subunit in L2/3 pyramidal neurons in the ACC in chronic pain (Wu and Zhuo, 2009). There, enhancement of GluN2B function is related to increased inflammatory pain responses (Wei et al., 2001; Wu et al., 2005) and the maintenance of neuropathic pain (Abe et al., 2005). Also, an interaction of GluN2B with caveolin has been described that promotes the development of chronic pain (Yang et al., 2015). Thus, it is difficult to derive therapeutic interventions in chronic pain based on modulation of the ubiquitously expressed GluN2B subunit that has diverse and opposing effects on synaptic plasticity in pathologic conditions (Yashiro and Philpot, 2008).

The finding that only synapses of projections from the ATN show the nerve injury-induced exclusion of the GluN2B-subunit is important for the potential functional role of this phenotype. ATN are composed of three distinct nuclei: the anterodorsal, anteroventral, and anteromedial nucleus. While all three of them project to different parts of the cingulate cortex, the ACC receives inputs mainly from the AM nucleus which is reciprocally connected to the ACC and the PFC (Jankowski et al., 2013). The ATN are implicated in the formation of emotion, and they are an integral part of the limbic system (Nishio et al., 2011). Their function in nociception and emotional aspects of pain has been demonstrated by chemogenetic activation of GABAergic inputs to the anterodorsal and paratenial thalamic nucleus, which mimics pain-induced hypersensitivity (Liu et al., 2017). In this light, our data suggest that the impairment of synaptic plasticity from ATN to the ACC contributes to altered nociceptive processing and presumably to the affective/emotional component of pain.

References

Abe T, Matsumura S, Katano T, Mabuchi T, Takagi K, Xu L, Yamamoto A, Hattori K, Yagi T, Watanabe M, Nakazawa T, Yamamoto T, Mishina M, Nakai Y, Ito S (2005) Fyn kinase-mediated phosphorylation of NMDA receptor NR2B subunit at Tyr1472 is essential for maintenance of neuropathic pain. Eur J Neurosci 22:1445–1454.

Barth AL, Poulet JF (2012) Experimental evidence for sparse firing in the neocortex. Trends Neurosci 35:345–355.

Basbaum AI, Bautista DM, Scherrer G, Julius D (2009) Cellular and molecular mechanisms of pain. Cell 139:267–284.

Bender VA, Bender KJ, Brasier DJ, Feldman DE (2006) Two coincidence detectors for spike timing-dependent plasticity in somatosensory cortex. J Neurosci 26:4166–4177.

Bi GQ, Poo MM (1998) Synaptic modifications in cultured hippocampal neurons: dependence on spike timing, synaptic strength, and postsynaptic cell type. J Neurosci 18:10464–10472.

Bliss TV, Collingridge GL, Kaang BK, Zhuo M (2016) Synaptic plasticity in the anterior cingulate cortex in acute and chronic pain. Nat Rev Neurosci 17:485–496.

Blom SM, Pfister JP, Santello M, Senn W, Nevian T (2014) Nerve injury-induced neuropathic pain causes disinhibition of the anterior cingulate cortex. J Neurosci 34:5754–5764.

Calejesan AA, Kim SJ, Zhuo M (2000) Descending facilitatory modulation of a behavioral nociceptive response by stimulation in the adult rat anterior cingulate cortex. Eur J Pain 4:83–96.

Casado M, Dieudonné S, Ascher P (2000) Presynaptic N-methyl-D-aspartate receptors at the parallel fiber-Purkinje cell synapse. Proc Natl Acad Sci USA 97:11593–11597.

Chen T, Wang W, Dong YL, Zhang MM, Wang J, Koga K, Liao YH, Li JL, Budisantoso T, Shigemoto R, Itakura M, Huganir RL, Li YQ, Zhuo M (2014a) Postsynaptic insertion of AMPA receptor onto cortical pyramidal neurons in the anterior cingulate cortex after peripheral nerve injury. Mol Brain 7:76.

Chen T, Koga K, Descalzi G, Qiu S, Wang J, Zhang LS, Zhang ZJ, He XB, Qin X, Xu FQ, Hu J, Wei F, Huganir RL, Li YQ, Zhuo M (2014b) Postsynaptic potentiation of corticospinal projecting neurons in the anterior cingulate cortex after nerve injury. Mol Pain 10:33.

Chiou CS, Huang CC, Liang YC, Tsai YC, Hsu KS (2012) Impairment of long-term depression in the anterior cingulate cortex of mice with bone cancer pain. Pain 153:2097–2108.

Christopherson KS, Hillier BJ, Lim WA, Bredt DS (1999) PSD-95 assembles a ternary complex with the N-methyl-D-aspartic acid receptor and a bivalent neuronal NO synthase PDZ domain. J Biol Chem 274:27467–27473.

Dan Y, Poo MM (2006) Spike timing-dependent plasticity: from synapse to perception. Physiol Rev 86:1033–1048.

Del Rey A, Yau HJ, Randolf A, Centeno MV, Wildmann J, Martina M, Besedovsky HO, Apkarian VA (2011) Chronic neuropathic pain-like behavior correlates with IL-1β expression and disrupts cytokine interactions in the hippocampus. Pain 152:2827–2835.

Egger V, Nevian T, Bruno RM (2008) Subcolumnar dendritic and axonal organization of spiny stellate and star pyramid neurons within a barrel in rat somatosensory cortex. Cereb Cortex 18:876–889.

Erreger K, Dravid SM, Banke TG, Wyllie DJ, Traynelis SF (2005) Subunit-specific gating controls rat NR1/NR2A and NR1/NR2B NMDA channel kinetics and synaptic signalling profiles. J Physiol 563:345–358.

Fillinger C, Yalcin I, Barrot M, Veinante P (2017) Afferents to anterior cingulate areas 24a and 24b and midcingulate areas 24a′ and 24b′ in the mouse. Brain Struct Funct 222:1509–1532.

Garthwaite J (2008) Concepts of neural nitric oxide-mediated transmission. Eur J Neurosci 27:2783–2802.

Hardingham N, Dachtler J, Fox K (2013) The role of nitric oxide in pre-synaptic plasticity and homeostasis. Front Cell Neurosci 7:190.

Huang CC, Hsu KS (2010) Activation of muscarinic acetylcholine receptors induces a nitric oxide-dependent long-term depression in rat medial prefrontal cortex. Cereb Cortex 20:982–996.

Jankowski MM, Ronnqvist KC, Tsanov M, Vann SD, Wright NF, Erichsen JT, Aggleton JP, O'Mara SM (2013) The anterior thalamus provides a subcortical circuit supporting memory and spatial navigation. Front Syst Neurosci 7:45.

Kang SJ, Liu MG, Chen T, Ko HG, Baek GC, Lee HR, Lee K, Collingridge GL, Kaang BK, Zhuo M (2012) Plasticity of metabotropic glutamate receptor-dependent long-term depression in the anterior cingulate cortex after amputation. J Neurosci 32:11318–11329.

Kasanetz F, Nevian T (2021) Increased burst coding in deep layers of the ventral anterior cingulate cortex during neuropathic pain. Sci Rep 11:24240.

Koga K, Descalzi G, Chen T, Ko HG, Lu J, Li S, Son J, Kim T, Kwak C, Huganir RL, Zhao MG, Kaang BK, Collingridge GL, Zhuo M (2015) Coexistence of two forms of LTP in ACC provides a synaptic mechanism for the interactions between anxiety and chronic pain. Neuron 85:377–389.

Kuner R (2010) Central mechanisms of pathological pain. Nat Med 16:1258–1266.

Li XY, Ko HG, Chen T, Descalzi G, Koga K, Wang H, Kim SS, Shang Y, Kwak C, Park SW, Shim J, Lee K, Collingridge GL, Kaang BK, Zhuo M (2010) Alleviating neuropathic pain hypersensitivity by inhibiting PKMzeta in the anterior cingulate cortex. Science 330:1400–1404.

Liu J, Zhang MQ, Wu X, Lazarus M, Cherasse Y, Yuan MY, Huang ZL, Li RX (2017) Activation of parvalbumin neurons in the rostro-dorsal sector of the thalamic reticular nucleus promotes sensitivity to pain in mice. Neuroscience 366:113–123.

Liu MG, Zhuo M (2014) Loss of long-term depression in the insular cortex after tail amputation in adult mice. Mol Pain 10:1.

Lourenco J, Pacioni S, Rebola N, van Woerden GM, Marinelli S, DiGregorio D, Bacci A (2014) Non-associative potentiation of perisomatic inhibition alters the temporal coding of neocortical layer 5 pyramidal neurons. PLoS Biol 12:e1001903.

Markram H, Lubke J, Frotscher M, Sakmann B (1997) Regulation of synaptic efficacy by coincidence of postsynaptic APs and EPSPs. Science 275:213–215.

Marti Mengual U, Wybo WA, Spierenburg LJ, Santello M, Senn W, Nevian T (2020) Efficient low-pass dendro-somatic coupling in the apical dendrite of layer 5 pyramidal neurons in the anterior cingulate cortex. J Neurosci 40:8799–8815.

Min R, Nevian T (2012) Astrocyte signaling controls spike timing-dependent depression at neocortical synapses. Nat Neurosci 15:746–753.

Nabavi S, Kessels HW, Alfonso S, Aow J, Fox R, Malinow R (2013) Metabotropic NMDA receptor function is required for NMDA receptor-dependent long-term depression. Proc Natl Acad Sci USA 110:4027–4032.

Neubauer FB, Min R, Nevian T (2022) Presynaptic NMDA receptors influence Ca^{2+} dynamics by interacting with voltage-dependent calcium channels during the induction of long-term depression. Neural Plasticity 2022:2900875.

Nevian T, Sakmann B (2004) Single spine Ca^{2+} signals evoked by coincident EPSPs and backpropagating action potentials in spiny stellate cells of layer 4 in the juvenile rat somatosensory barrel cortex. J Neurosci 24:1689–1699.

Nevian T, Sakmann B (2006) Spine Ca^{2+} signaling in spike-timing-dependent plasticity. J Neurosci 26:11001–11013.

Nishio Y, Hashimoto M, Ishii K, Mori E (2011) Neuroanatomy of a neurobehavioral disturbance in the left anterior thalamic infarction. J Neurol Neurosurg Psychiatry 82:1195–1200.

Ossipov MH, Morimura K, Porreca F (2014) Descending pain modulation and chronification of pain. Curr Opin Support Palliat Care 8:143–151.

Paoletti P, Bellone C, Zhou Q (2013) NMDA receptor subunit diversity: impact on receptor properties, synaptic plasticity and disease. Nat Rev Neurosci 14:383–400.

Park L, Hochrainer K, Hattori Y, Ahn SJ, Anfray A, Wang G, Uekawa K, Seo J, Palfini V, Blanco I, Acosta D, Eliezer D, Zhou P, Anrather J, Iadecola C (2020) Tau induces PSD95-neuronal NOS uncoupling and neurovascular dysfunction independent of neurodegeneration. Nat Neurosci 23:1079–1089.

Reyes A, Lujan R, Rozov A, Burnashev N, Somogyi P, Sakmann B (1998) Target-cell-specific facilitation and depression in neocortical circuits. Nat Neurosci 1:279–285.

Rodriguez-Moreno A, Gonzalez-Rueda A, Banerjee A, Upton AL, Craig MT, Paulsen O (2013) Presynaptic self-depression at developing neocortical synapses. Neuron 77:35–42.

Sandkuhler J (2000) Learning and memory in pain pathways. Pain 88:113–118.

Santello M, Bisco A, Nevian NE, Lacivita E, Leopoldo M, Nevian T (2017) The brain-penetrant 5-HT7 receptor agonist LP-211 reduces the sensory and affective components of neuropathic pain. Neurobiol Dis 106:214–221.

Santello M, Nevian T (2015) Dysfunction of cortical dendritic integration in neuropathic pain reversed by serotoninergic neuromodulation. Neuron 86:233–246.

Sellmeijer J, Mathis V, Hugel S, Li XH, Song Q, Chen QY, Barthas F, Lutz PE, Karatas M, Luthi A, Veinante P, Aertsen A, Barrot M, Zhuo M, Yalcin I (2018) Hyperactivity of anterior cingulate cortex areas 24a/24b drives chronic pain-induced anxiodepressive-like consequences. J Neurosci 38:3102–3115.

Sieber AR, Min R, Nevian T (2013) Non-Hebbian long-term potentiation of inhibitory synapses in the thalamus. J Neurosci 33:15675–15685.

Sjostrom PJ, Turrigiano GG, Nelson SB (2001) Rate, timing, and cooperativity jointly determine cortical synaptic plasticity. Neuron 32:1149–1164.

Sjostrom PJ, Turrigiano GG, Nelson SB (2003) Neocortical LTD via coincident activation of presynaptic NMDA and cannabinoid receptors. Neuron 39:641–654.

Sobczyk A, Scheuss V, Svoboda K (2005) NMDA receptor subunit-dependent [Ca2+] signaling in individual hippocampal dendritic spines. J Neurosci 25:6037–6046.

Tsumoto T (1993) Long-term depression in cerebral cortex: a possible substrate of 'forgetting' that should not be forgotten. Neurosci Res 16:263–270.

van Huijstee AN, Kessels HW (2020) Variance analysis as a tool to predict the mechanism underlying synaptic plasticity. J Neurosci Methods 331:108526.

Vicini S, Wang JF, Li JH, Zhu WJ, Wang YH, Luo JH, Wolfe BB, Grayson DR (1998) Functional and pharmacological differences between recombinant N-methyl-D-aspartate receptors. J Neurophysiol 79:555–566.

Wei F, Li P, Zhuo M (1999) Loss of synaptic depression in mammalian anterior cingulate cortex after amputation. J Neurosci 19:9346–9354.

Wei F, Wang GD, Kerchner GA, Kim SJ, Xu HM, Chen ZF, Zhuo M (2001) Genetic enhancement of inflammatory pain by forebrain NR2B overexpression. Nat Neurosci 4:164–169.

Woolf CJ (1983) Evidence for a central component of post-injury pain hypersensitivity. Nature 306:686–688.

Woolf CJ, Salter MW (2000) Neuronal plasticity: increasing the gain in pain. Science 288:1765–1769.

Wu LJ, Toyoda H, Zhao MG, Lee YS, Tang J, Ko SW, Jia YH, Shum FW, Zerbinatti CV, Bu G, Wei F, Xu TL, Muglia LJ, Chen ZF, Auberson YP, Kaang BK, Zhuo M (2005) Upregulation of forebrain NMDA NR2B receptors contributes to behavioral sensitization after inflammation. J Neurosci 25:11107–11116.

Wu LJ, Zhuo M (2009) Targeting the NMDA receptor subunit NR2B for the treatment of neuropathic pain. Neurotherapeutics 6:693–702.

Xu H, Wu LJ, Wang H, Zhang X, Vadakkan KI, Kim SS, Steenland HW, Zhuo M (2008) Presynaptic and postsynaptic amplifications of neuropathic pain in the anterior cingulate cortex. J Neurosci 28:7445–7453.

Yang JX, Hua L, Li YQ, Jiang YY, Han D, Liu H, Tang QQ, Yang XN, Yin C, Hao LY, Yu L, Wu P, Shao CJ, Ding HL, Zhang YM, Cao JL (2015) Caveolin-1 in the anterior cingulate cortex modulates chronic neuropathic pain via regulation of NMDA receptor 2B subunit. J Neurosci 35:36–52.

Yashiro K, Philpot BD (2008) Regulation of NMDA receptor subunit expression and its implications for LTD, LTP, and metaplasticity. Neuropharmacology 55:1081–1094.

Zhou L, Zhu DY (2009) Neuronal nitric oxide synthase: structure, subcellular localization, regulation, and clinical implications. Nitric Oxide 20:223–230.

Zhuo M (2008) Cortical excitation and chronic pain. Trends Neurosci 31:199–207.